Freely-migrating-defect production during irradiation at elevated temperatures

T. Hashimoto
Energy Research Laboratory, Hitachi Ltd., 1168 Moriyamacho, Hitachi, Ibaraki 316, Japan

L. E. Rehn and P. R. Okamoto
Materials Science Division, Argonne National Laboratory, Argonne, Illinois 60439
(Received 15 August 1988)

Radiation-induced segregation in a Cu–1 at. % Au alloy was investigated using *in situ* Rutherford backscattering spectrometry. The amount of Au atom depletion in the near surface region was measured as a function of dose during irradiation at 350 °C with four ions of substantially different masses. Relative efficiencies for producing freely migrating defects were evaluated for 1.8-MeV ^{1}H, ^{4}He, ^{20}Ne, and ^{84}Kr ions by determining beam current densities that gave similar radiation-induced segregation rates. Irradiations with primary knock-on atom median energies of 1.7, 13, and 79 keV yielded relative efficiencies of 53, 7, and 6 %, respectively, compared to the irradiation with a 0.83-keV median energy. Despite quite different defect and host alloy properties, the relative efficiencies for producing freely migrating defects determined in Cu-Au are remarkably similar to those found previously in Ni-Si alloys. Hence, the reported efficiencies appear to offer a reliable basis for making quantitative correlations of microstructural changes induced in different alloy systems by a wide variety of irradiation particles.

I. INTRODUCTION

Ion irradiation is used to study irradiation effects in fission and fusion reactor materials because of its high degree of flexibility in achieving various irradiation conditions. To obtain the full benefit from such studies, a capability must be developed for making quantitative correlations of microstructural changes produced in different irradiation environments. Quantitative correlations of such microstructural changes are also needed in order to predict materials behavior in irradiation environments that currently do not exist, but are anticipated for future development.

Many microstructural changes that occur during irradiation at elevated temperatures are caused primarily by those defects that survive recombination and/or clustering in the cascade region and become free to migrate long distances. Hence, the net production rate of these freely migrating defects must be known for different irradiation particles and energies before quantitative correlations can be made of microstructural changes that occur at elevated temperatures, e.g., void swelling, irradiation creep, radiation-induced segregation, and precipitation, as well as the dissolution of existing metastable phases and concentration gradients.

Measurements of irradiation-induced resistivity changes at low temperatures[1] have been used to estimate defect production efficiencies for several years. However, no systematic studies of defect production efficiencies as a function of primary-recoil energy at temperatures above room temperature were available until recently. Okamoto *et al.*[2] have shown that the relative efficiencies of different ions for producing freely migrating defects at elevated temperatures can be determined from measurements of radiation-induced segregation (RIS), because RIS is caused only by those defects that escape from their parent cascade and become free to migrate long distances. RIS occurs because, in general, vacancy and/or interstitial defects in alloys preferentially migrate via particular elemental components. This preferential coupling of some alloying components to the persistent defect fluxes generated during irradiation causes segregation by sweeping certain elements into, and other elements out of, local regions which experience a net influx or outflow of defects, e.g., near grain boundaries, dislocations, and the external surface.

Systematic studies of RIS have been carried out on several Ni-based binary alloys.[3–5] In solid-solution Ni-Si alloys, irradiation at elevated temperatures produced nonequilibrium coatings of the Ni_3Si phase on the surfaces. Details of the Ni_3Si coating growth kinetics were established using *in situ* Rutherford backscattering spectrometry (RBS).[3] During irradiations at similar calculated defect production rates, a strong decrease in the measured coating growth rate was found with increasing ion mass.[6] These measurements, and the understanding of the coating growth kinetics that was demonstrated, were used to[7] determine the relative efficiencies of several different ion species for producing freely migrating defects in Ni-Si alloys. It was found that heavy-ion irradiations are only a few percent as efficient as light-ion irradiations for producing freely migrating defects. The strong decrease in efficiency with increasing ion mass is consistent with more limited experimental observations reported previously under fast and thermal neutron irradiation.[8]

In order to examine the universality of the defect production efficiencies found for Ni-Si alloys, we have investigated RIS in Cu–1 at. % Au alloys using *in situ* RBS.[9] The major reasons for selecting a Cu-Au alloy are (1)

Considerable thermal diffusion and irradiation data are available for Cu-Au; (2) the transport of solute during irradiation is expected to be different in Ni-Si and Cu-Au alloys because Au is an oversized atom in Cu, whereas Si is undersized in Ni; and (3) the alloy is well suited for RBS because signals from the heavier Au atoms in the near-surface region are well separated from signals of the more abundant Cu atoms. Hence, (4) quantitative measurements of segregation can be made in very dilute alloys, where precipitation effects are minimized.

In Ref. 9, we reported experimental measurements of RIS in Cu–1 at. % Au alloys produced under 1.8-MeV He irradiation, and the theoretical analysis of the segregation kinetics. In this paper, we report the relative efficiences of several additional ions for producing freely migrating defects that were determined from measurements of RIS kinetics in Cu–1 at. % Au at elevated temperature. The modeling and verification of the RIS kinetics that are necessary to extract efficiencies from the measurements are presented in Sec. II. The relative efficiencies are evaluated in Sec. III, and various implications of the present results are discussed in Sec. IV.

II. KINETICS OF RIS IN Cu-Au ALLOYS

The kinetics of RIS in Cu–1 at. % Au alloys was investigated using RBS.[9] In this section, the experimental results and theoretical analysis of the segregation kinetics are presented. The experimental procedures are similar to those used for Ni-Si alloys and the details are described in Ref. 4. The cross section for Frenkel pair production in the near-surface region was computed using the PINTO program,[10] and the resulting value was then used to convert the measured ion-beam current density into a corresponding displacement rate. Pure Cu and an average displacement energy of 29 eV were assumed for these calculations.

Experimentally, a sequence of RBS spectra is acquired as a function of time during ion irradiation at a constant dose rate. Difference spectra are then obtained by subtracting each subsequent spectrum from the initial spectrum. Figure 1(a) shows a series of RBS spectra acquired during 1.8-MeV He irradiation, at 350 °C, and the difference spectra are displayed in Fig. 1(b). These difference spectra clearly show that irradiation of Cu-Au at elevated temperatures causes depletion of Au atoms in the near-surface region. Annealing of the specimens at the same temperature in the absence of irradiation returned the alloy composition to its original uniform state, demonstrating that the Au depletion was truly radiation induced, and not simply a result of enhanced diffusivity during irradiation. Less than two atom layers are removed by sputtering during the course of these experiments. Furthermore, as is discussed later in this section, the assumption that preferential sputtering of Au is responsible for the Au depletion yields dose-rate-dependent kinetics which contradict the experimental results. Hence, all sputter-induced compositional changes can be neglected. The total decrease in the RBS yield from Au in the near-surface depleted region, M, which is directly proportional to the amount of RIS, was measured as a function of dose, dose rate, and temperature. RIS was observed in the temperature range between about 300 and 500 °C. Figure 2 shows the amount of Au depletion measured as a function of dose during 1.8-MeV He irradiation at five different temperatures for a calculated displacement rate of 3.9×10^{-5} dpa/s (dpa stands for displacements per atom). The segregation rate peaks near 400 °C.

One reason for selecting Cu-Au for the present experiment was that a considerable amount of information already exists on diffusion in this alloy in the absence of irradiation, i.e., where vacancy jumps dominate mass

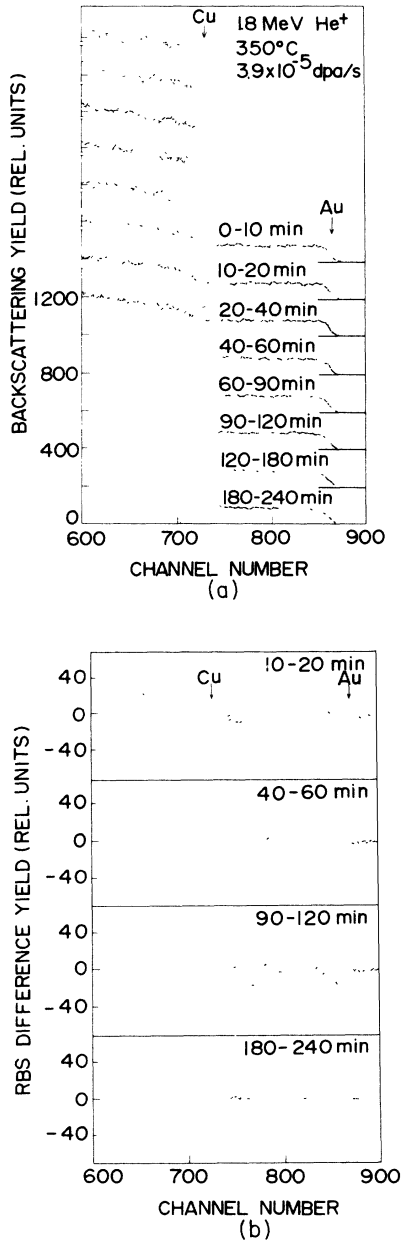

FIG. 1. (a) Series of RBS spectra acquired during 1.8-MeV He irradiation. The time intervals indicate the collection period. (b) Difference spectra for the RBS spectra in (a) (Ref. 9).

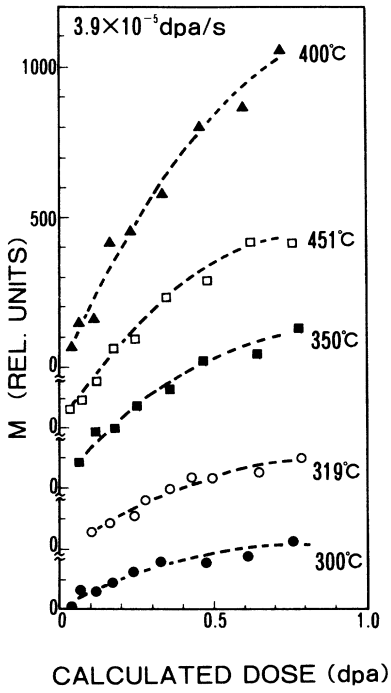

FIG. 2. Amount of near-surface, Au atom depletion measured by RBS during 1.8-MeV He irradiation at five different temperatures (Ref. 9).

transport. The effect of vacancy fluxes on Au transport during irradiation can be predicted using this existing data. Hirano has analyzed the diffusion results in dilute Cu-Au alloys in terms of the five-frequency jump model,[11] and determined that the ratios ω_4/ω_0 and ω_2/ω_1 are both smaller than unity.[12] In the five-frequency model, ω_0 is the jump frequency for exchange of a Cu atom with a vacancy which is far away from a Au atom, and ω_4 is the frequency of a vacancy jump onto one of the first-neighbor sites with the Au. The fact that $\omega_4/\omega_0 < 1$ indicates Au atoms are, in general, repelled from vacancies in Cu-Au. Therefore, Au-vacancy complexes, which would produce enrichment of Au at the surface during irradiation, do not form. In the model, ω_2 is the jump frequency for exchange of a vacancy with a Au atom, and ω_1 is the frequency for Cu-vacancy jumps between first-nearest neighbors of a Au atom. Hence, $\omega_2/\omega_1 < 1$ means Cu diffuses faster via vacancies than Au does.

During irradiation, a vacancy and an interstitial flux are created that both flow toward the surface. The analysis in the previous paragraph shows that the vacancy flux will preferentially transport Cu atoms away from the surface, i.e., that the vacancy flux will induce Au enrichment at the surface. Since Au depletion was observed during irradiation, preferential transport of Cu atoms toward the surface by the interstitial flux apparently dominates over the vacancy-induced Au enrichment contribution to RIS in Cu-Au alloys. This can be understood as follows. Au is an oversized solute atom in Cu. Self-interstitial atoms trapped near oversized solute atoms will dissociate and migrate via an interstitialcy mechanism rather than as an interstitial-solute complex.[13] In this manner, solvent (Cu) atoms are preferentially transported toward the surface by the interstitial flux, producing the observed depletion of Au. Hence, the defect mechanism responsible for RIS in Cu-Au is apparently different from that in Ni-Si alloys, where preferential transport of solute is believed to occur via the formation and migration of interstitial-Si complexes.[5]

Figure 3 is a schematic of the Au atom concentration profile generated near the surface during irradiation. The amount of segregation measured in the experiments is defined to be $M(t)$, where

$$M(t)=\int_0^{l(t)}[C_{\mathrm{Au}}^0-C_{\mathrm{Au}}(x,t)]dx \ . \tag{1}$$

Here, $l(t)$ is the depth of the Au depleted region, $C_{\mathrm{Au}}(x,t)$ is the Au atom concentration as a function of depth, x, and time, t, during irradiation, and C_{Au}^0 is the initial uniform Au concentration. The segregation rate is related to the solute (Au) flux, $J_{\mathrm{Au}}(l)$, toward the surface by

$$\frac{dM(t)}{dt}=J_{\mathrm{Au}}(l) \ . \tag{2}$$

According to the argument given above, the interstitial flux generated toward the surface during irradiation preferentially drives Cu atoms toward the surface, while the vacancy flux preferentially transport Au atoms toward the surface. Taking backdiffusion down the induced solute concentration gradient into consideration, the flux of Au atoms, J_{Au}, out of the near-surface region during irradiation can therefore be written according to the Johnson-Lam model[14] as

$$J_{\mathrm{Au}}=k_I C_{\mathrm{Au}} D_I \nabla C_I - k_V C_{\mathrm{Au}} D_V \nabla C_V - (k_B D_I C_I + k_B' D_V C_V)\nabla C_{\mathrm{Au}} \ , \tag{3}$$

where D_I and D_V are, respectively, the diffusion coefficients for interstitials and vacancies, whose concentrations are given by C_I and C_V. k_I, k_V, k_B, and k_B' are the phenomenological defect-solute coupling

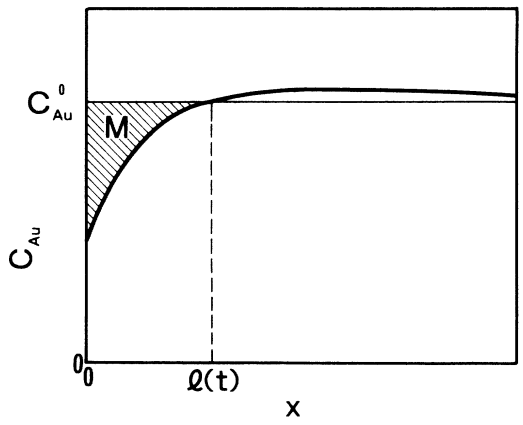

FIG. 3. Schematic diagram of the Au atom concentration profile in the near-surface region (Ref. 9).

coefficients.[9] We assume that C_I and C_V attain steady state quickly and remain time independent during irradiation. Numerical calculations based on the Johnson-Lam model[14] show that indeed, C_I and C_V attain their steady-state values after only about 1 s of irradiation. Steady-state solutions for C_I and C_V have been given by Lam *et al.*[15] Here we employ their solutions for the uniform irradiation of a semi-infinite slab at low temperatures, where the thermal equilibrium defect concentrations are negligible. Substituting $dt = d\phi/K_0$ for irradiation at a constant dose rate, K_0, we obtain

$$\frac{dM}{d\phi} = \frac{1}{\sqrt{2}} \left[\frac{D_I D_V}{K_0 K_1} \right]^{1/4} \frac{(1+S)^{1/2}}{(1+2S)^{3/4}} \times \left[(k_I - k_V) \left[\frac{dY}{dX} \right]_{X=L} C_{\mathrm{Au}}^0 - (k_B + k_B')Y(L) \left[\frac{\partial C_{\mathrm{Au}}}{\partial X} \right]_{X=L} \right], \quad (4)$$

where

$$Y(X) = 1 - \frac{12A(S+1)}{[A\exp(X) + \exp(-X)]^2},$$

$$X = \left[\frac{K_0 K_1}{D_I D_V} \right]^{1/4} \left[\frac{1+S}{2(1+2S)^{1/2}} \right]^{1/2} x,$$

$$A = 5 + 6S + [(5+6S)^2 - 1]^{1/2},$$

$$L(t) = \left[\frac{K_0 K_1}{D_I D_V} \right]^{1/4} \left[\frac{1+S}{2(1+2S)^{1/2}} \right]^{1/2} l(t).$$

K_0 is the actual atomic displacement rate, K_1 is the rate coefficient for mutual recombination of vacancies and interstitials, S is the generalized sink concentration as defined by Lam *et al.*,[15] X is the dimensionless distance from the surface, and L is the dimensionless depth of the Au depleted region. $S \ll 1$ means that most of the defects are lost through recombination of vacancy and interstitial defects (recombination-limited regime), whereas $S \gg 1$ means that most of the defects annihilate at fixed sinks (sink-dominant regime).

Expanding $Y(X)$ in a series and integrating, we obtain

$$M = p\phi + \cdots \quad (5)$$

where the ellipsis represents higher-order terms in ϕ and

$$p = \sqrt{2}(k_I - k_V) \frac{(1+S)^{1/2}}{(1+2S)^{3/4}} \frac{A(12S+9)-1}{A(12S+11)-1} \times \left[\frac{D_I D_V}{K_0 K_1} \right]^{1/4} C_{\mathrm{Au}}^0.$$

Equations (4) and (5) predict the following dose dependence for M. M is directly proportional to the dose in the early stages of irradiation; at intermediate doses M increases less than linearly with dose mainly due to the effect of backdiffusion; at high doses, when the segregation and backdiffusion terms balance, M becomes constant. Figure 4 shows a result of numerical calculations

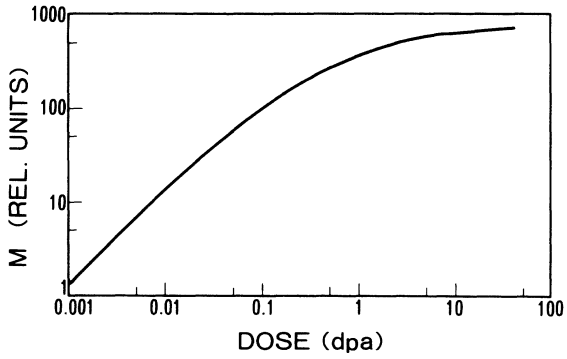

FIG. 4. Dose dependence of the amount of segregation obtained by the numerical calculations using the Johnson-Lam model (Ref. 9). Input parameters used in the calculation are listed in Table II.

of M using the Johnson-Lam model, which confirms these predictions for an irradiation temperature of 350 °C and a displacement rate of 3.9×10^{-5} dpa/s. Note that the experimental results shown in Fig. 2 also exhibit this predicted dose dependence.

Further, numerical calculations using the Johnson-Lam model reveal that the dimensionless depth of the depleted region, L, and the solute concentration as a function of dimensionless distance, $C_{\mathrm{Au}}(X)$, both exhibit only a weak dependence on dose rate when evaluated at a fixed dose. This is explained as follows. If mutual recombination is the dominant mechanism of defect annihilation ($S \ll 1$), p in Eq. (5) is larger at a given dose for irradiation at a lower dose rate because of the $-\frac{1}{4}$ power dependence of p on dose rate. Consequently, M, and the depletion depth, l, are also larger for a lower dose rate. This mitigates the dose-rate dependence of L, because L is proportional to $K_0^{1/4} l$. If sinks dominate defect annihilation ($S \gg 1$), each defect migrates the same average distance regardless of dose rate and Eq. (5) then predicts that M becomes independent of dose rate. Consequently L is also independent of dose rate for $S \gg 1$.

$Y(X)$ in Eq. (4) is a dimensionless function that mirrors the depth profile of interstitials and vacancies.[15] $Y(X)$ does not depend explicitly on dose rate, but only implicitly through its dependence on X. The Au concentration profile, $C_{\mathrm{Au}}(X)$, also depends on dose rate only implicitly through its dependence on X. Since L is independent of dose rate, $(dY/dX)_{X=L}$, $Y(L)$, and $(\partial C_{\mathrm{Au}}/\partial X)_{X=L}$ in Eq. (4) are also independent of dose rate. Hence, the quantity within large square brackets in Eq. (4) is independent of the dose rate. When $S \ll 1$, the dose rate dependence of $dM/d\phi$ is determined only by the factor $K_0^{-1/4}$. The other factors in Eq. (4) do not depend on dose rate, but only on the dose. Therefore, we include all factors other than $K_0^{-1/4}$ in $F(\phi)$.

When $S \gg 1$, S is proportional to K_0.[15] In this case, the dose-rate dependence of $dM/d\phi$ is determined by the factors $K_0^{-1/4}$ and $(1+S)^{1/2}(1+2S)^{-3/4} \sim S^{-1/4}$. Since $S \propto K_0^{-1}$, the product $K_0^{-1/4} S^{-1/4}$ becomes independent of dose rate. Therefore, all the factors in Eq. (4) do not

depend on dose rate, and can be written together as $G(\phi)$. Writing the dose rate dependence of $dM/d\phi$ explicitly, one obtains

$$\frac{dM}{d\phi}=\begin{cases}F(\phi)K_0^{-1/4} & (S\ll 1)\\ G(\phi) & (S\gg 1)\,.\end{cases} \tag{6}$$

Hence the ratio, R, of measurements of $dM/d\phi$ for two irradiations at different dose rates, $K_{0,1}$ and $K_{0,2}$, equals

$$R=\frac{(dM/d\phi)_1}{(dM/d\phi)_2}=\begin{cases}\left[\dfrac{K_{0,1}}{K_{0,2}}\right]^{-1/4} & (S\ll 1)\\ 1 & (S\gg 1)\,.\end{cases} \tag{7}$$

If we assume that preferential sputtering of Au is responsible for the Au depletion observed in the near-surface region, Eq. (2) is replaced by

$$\frac{dM}{dt}=J_{\mathrm{Au}}^{\mathrm{sp}}\,, \tag{8}$$

where, $J_{\mathrm{Au}}^{\mathrm{sp}}$ is the loss of Au atoms by sputtering. Since $J_{\mathrm{Au}}^{\mathrm{sp}}$ is proportional to $K_0C_{\mathrm{Au}}(0,t)$, dM/dt becomes proportional to $C_{\mathrm{Au}}(0,t)$. Initially $C_{\mathrm{Au}}(0,t)$ is constant, and therefore,

$$M\propto\phi \tag{9}$$

will hold. Equation (9) predicts a similar dependence of M on dose as that in Eq. (5), which was confirmed experimentally. However, $dM/d\phi$ becomes independent of dose rate, because any sputter-induced change of $C_{\mathrm{Au}}(0,t)$ is independent of K_0 for a fixed dose. Hence,

$$R=1 \tag{10}$$

will hold.

Figure 5 shows experimental results for two different 366 °C irradiations with 1.8-MeV He at calculated dose rates of 6.4×10^{-6} and 9.6×10^{-5} dpa/s. The experimental data were first fitted by a least-squares procedure to a quadratic polynomial. The ratio R was then evaluated over the range where the experimental data overlap using

$$R_{\mathrm{expt}}=\frac{M_1(\phi_1)-M_1(\phi_0)}{M_2(\phi_1)-M_2(\phi_0)}\,. \tag{11}$$

The R_{expt} obtained for the data in Fig. 5 is 1.9 for doses between 0.1 and 0.15 dpa, in good agreement with the prediction for the recombination-limited regime from Eq. (7) of 2.0. We therefore conclude that the observed Au depletion cannot be attributed to the preferential sputtering of Au, and that mutual recombination is the dominant mechanism of defect annihilation during these He irradiations.

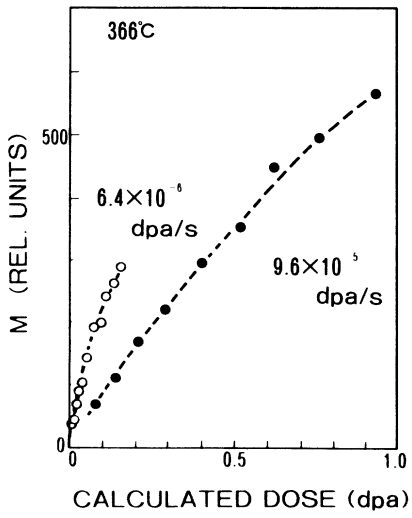

FIG. 5. Amount of segregation measured during 1.8-MeV He irradiation with two different dose rates (Ref. 9).

III. RELATIVE EFFICIENCIES FOR PRODUCING FREELY MIGRATING DEFECTS

The understanding of the RIS kinetics demonstrated in Sec. II provides a basis for determining the efficiencies of different irradiation particles for producing freely migrating defects in dilute Cu-Au alloys. Defining the efficiency, ϵ, for producing freely migrating defects as

$$\epsilon=\frac{K_0}{K_{\mathrm{calc}}}\,, \tag{12}$$

where K_0 is the actual production rate of freely migrating defects and K_{calc} is the calculated defect production rate, the relative efficiency, $\bar{\epsilon}$, of two different irradiation particles 1 and 2 becomes

$$\bar{\epsilon}=\frac{\epsilon_2}{\epsilon_1}=\frac{K_0^{(2)}/K_{\mathrm{calc}}^{(2)}}{K_0^{(1)}/K_{\mathrm{calc}}^{(1)}}\,, \tag{13}$$

Since only freely migrating defects contribute to RIS, the relative efficiency can be obtained by determining experimentally that beam current density for particle 2 which produces the same segregation rate as particle 1. Because $K_0^{(1)}$ equals $K_0^{(2)}$ for irradiations that produce the same segregation rate, the efficiency of particle 1 relative to particle 2 for producing freely migrating defects becomes

$$\bar{\epsilon}=\frac{K_{\mathrm{calc}}^{(1)}}{K_{\mathrm{calc}}^{(2)}}\,. \tag{14}$$

It should be emphasized that this method for determining relative production efficiencies for freely migrating defects does not depend on details of the RIS model, because segregation rates for different irradiation particles are compared directly. Therefore, this method is applicable to all alloy systems in which RIS occurs, regardless of the segregation kinetics.

Instead of performing many measurements varying the beam current density until the same segregation rate is attained, an alternative method based on the known dose-rate dependence discussed in Sec. II can be utilized in the Cu-Au alloy. From the observed $-\frac{1}{4}$ power dependence of M on dose rate, the data points obtained

with particle 2, $(\phi^{(2)},M^{(2)})$, will fall onto the same curve as those of particle 1, $M^{(1)}(\phi)$, when they are transformed in the following fashion:

$$(\phi^{(2)},M^{(2)})\rightarrow(\bar{\epsilon}\phi^{(2)},(\bar{\epsilon}K^{(2)}_{\rm calc}/K^{(1)}_{\rm calc})^{1/4}M^{(2)}) . \quad (15)$$

Therefore, $\bar{\epsilon}\equiv\epsilon_2/\epsilon_1$ can be determined by a least-squares-fitting method in which

$$\Delta^2=\sum_i\left[\left[\frac{\bar{\epsilon}K^{(2)}_{\rm calc}}{K^{(1)}_{\rm calc}}\right]^{1/4}M_i^{(2)}-M^{(1)}(\bar{\epsilon}\phi_i^{(2)})\right]^2 \quad (16)$$

is minimized; here i denotes individual data points measured during irradiation with particle 2. Any errors are minimized, of course, when the actual experimental segregation rates for the two different irradiations are as close as possible.

The amount of RIS in Cu–1 at. % Au during 1.8-MeV H, He, Ne, or Kr irradiation was measured as a function of irradiation dose at 350 °C. This temperature is ~50 °C below the maximum segregation temperature, consistent with the approximations discussed in deriving Eq. (7). Beam current densities, cross sections for Frenkel pair production calculated using the PINTO program, $\sigma_{\rm FP}$, and corresponding calculated dose rates in the near-surface region ($\leq$ 10 nm) are listed in Table I. Segregation during H and He irradiation was measured by simultaneously acquiring RBS spectra from the backscattered particles. The amount of segregation obtained from the H spectra was correlated to that from the He spectra using our RBS simulation program,[16] which is based on an earlier program by Ziegler *et al.*[17] The conversion coefficient was also checked experimentally by analyzing with a He beam after the H irradiation. Very good agreement of the H and He analyses was found between the two procedures. For Ne and Kr irradiations, the specimens were irradiated at 350 °C and subsequently analyzed by RBS with a He beam at a temperature of 200 °C, where no additional segregation or annealing occurs.

To obtain correct relative efficiencies for the heavy ions, it was found necessary to account for the different damage rate distributions produced by light and heavy ions. Figure 6 shows damage rate distributions for 1.8-MeV He, Ne, and Kr ions calculated using the TRIM program,[18] assuming a pure Cu specimen with a threshold displacement energy of 29 eV. The depth of the Au depletion from RIS during the experiments was always less than 100 nm. Although the damage production during the H and He irradiations is quite uniform to depths

TABLE I. Irradiation parameters. All ions had 1.8 MeV irradiation energy.

Ion	$\sigma_{\rm FP}$ (cm^2)	I (μA/cm^2)	$K_{\rm calc}$ (dpa/s)
^{1}H	4.8×10^{-20}	17	5.0×10^{-6}
^{4}He	8.1×10^{-19}	7.6	3.9×10^{-5}
^{20}Ne	7.1×10^{-17}	0.15	6.7×10^{-5}
^{20}Ne	7.1×10^{-17}	0.45	2.0×10^{-4}
^{84}Kr	1.7×10^{-15}	0.038	4.0×10^{-4}

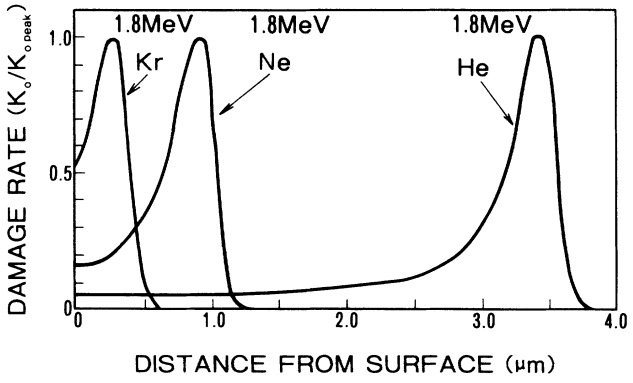

FIG. 6. Damage-rate distributions calculated by the TRIM program: (1) 1.8-MeV ^{4}He, (2) 1.8-MeV ^{20}Ne, (3) 1.8-MeV ^{84}Kr.

$\gtrsim$ 500 nm, it is not during the Ne and Kr irradiations. Numerical calculations using the Johnson-Lam model were employed to investigate the effect of the nonuniform defect production during Ne or Kr irradiation. Parameters used in the calculations are summarized in Table II. Figure 7 compares the results calculated using a uniform damage rate distribution, and using nonuniform profiles corresponding to Ne and Kr irradiations. The damage rates are all normalized to 4×10^{-5} dpa/s at the surface, because the He irradiation data will be used for particle 1 in Eq. (16).

The segregation rate, $dM/d\phi$, *calculated* numerically for 1.8-MeV Ne irradiation, was equal to that obtained with a uniform damage profile up to about 0.5 dpa. The rate became larger for Ne at higher doses. The equality of $dM/d\phi$ at lower doses occurs because the damage profile for Ne is essentially uniform with depth near the surface ($\lesssim$ 100 nm). However, for doses higher than about 0.5 dpa, the Au depleted region extends beyond 100 nm, where ∇C_I becomes larger for the Ne irradiation than for a uniform damage profile, providing a greater driving force for RIS. For 1.8-MeV Kr irradiation, the

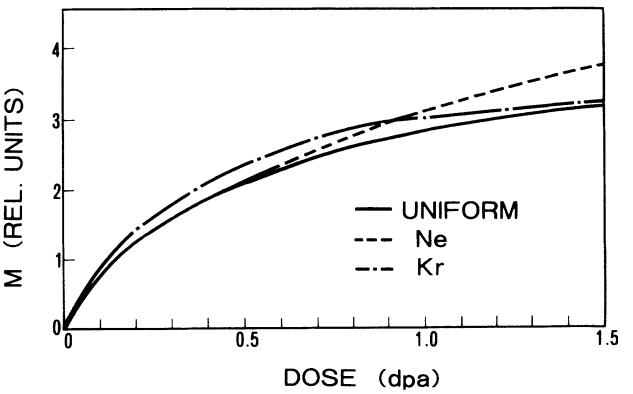

FIG. 7. Amount of segregation calculated for three different damage-rate distributions: (1) uniform, (2) 1.8-MeV Ne irradiation, (3) 1.8-MeV Kr irradiation.

TABLE II. Input parameters for the numerical calculations.

Parameter	Notation	Value	Refs. and remarks
Vibration frequency factor for interstitial	ν_I	5×10^{12} s^{-1}	19,20
Vibration frequency factor for vacancy	ν_V	5×10^{13} s^{-1}	19,21
Vibration frequency factor for type-*a* interstitial-solute complex	ν_{Iia}	5×10^{12} s^{-1}	19 ($\nu_{Iia}\sim\nu_I$)
Vibration frequency factor for vacancy-solute complex	ν_{Vi}	5×10^{13} s^{-1}	19($\nu_{Vi}\sim\nu_V$)
Formation energy of interstitial	H_I^F	2.2 eV	22
Formation energy of vacancy	H_V^F	1.3 eV	23,24
Migration energy of interstitial	H_I^M	0.12 eV	25
Migration energy of vacancy	H_V^M	0.76 eV	23,24
Migration energy of type-*a* interstitial-solute complex	H_{Iia}^M	0.148 eV	14 ($H_{Iia}^M=H_I^M-\frac{1}{5}H_{Iia}^B$)
Migration energy of vacancy-solute complex	H_{Vi}^M	0.76 eV	14 ($H_{Vi}^M=H_V^M$)
Binding energy of type-*a* interstitial-solute complex	H_{Iia}^B	−0.14 eV	assumed[a]
Binding energy of vacancy-solute complex	H_{Vi}^B	0.032 eV	assumed[a]
Initial solute concentration	C_i^0	10^{-2}	

[a]In the formulation of the Johnson-Lam model, the phenomenological coefficients, k_I and k_V, in Eq. (3) are related to the parameters of the "defect-solute complex" by $k_I=1-\exp\{[-(H_{Iia}^M-H_I^M)+H_{Iia}^B]/kT\}$ and $k_V=\exp\{[-(H_{Vi}^M-H_V^M)+H_{Vi}^B]/kT\}-1$ for the case of weak defect-solute binding as in Cu-Au alloys. The term "defect-solute complex" does not necessarily mean a physically discrete entity in this case (Ref. 9). The parameters were chosen so that k_I and k_V are positive and thus Au atom depletion will be simulated at the surface. When the ratio of M is taken as defined in Sec. III, uncertainty in these parameters cancel.

calculated $dM/d\phi$ was 12% higher than that for the uniform damage profile up to about 0.5 dpa due to the larger ∇C_I for the nonuniform Kr damage profile. However, the ratio of the segregation rate during the Kr irradiation to that of the uniform damage profile began to decrease near 0.5 dpa. Eventually, $dM/d\phi$ for Kr even became negative (not shown in Fig. 7). This is explained as follows. Since ∇C_I is negative beyond the damage peak, Au atoms flow toward the surface from behind the damage peak [see Eq. (3)]. Consequently, the total number of Au atoms is increasing with irradiation dose in the near-surface region in front of the damage peak. Since M is defined as the difference from the initial Au concentration [see Eq. (1)], the segregation rate decreases for doses $\gtrsim 0.5$ dpa. At very high doses, when the effect of the additional Au flowing from behind the damage peak becomes significant, $dM/d\phi$ eventually becomes negative. Another example of the effect of solute flowing toward the surface from behind the damage peak can be seen in Fig. 8 of Ref. 19. No decrease in the segregation rate was observed during Ne irradiation for the dose range (0–1.5 dpa) shown in Fig. 7. No decrease is, in fact, expected for the Ne, because the damage peak is considerably deeper than it is for Kr.

We, therefore, applied Eq. (16) to the Ne irradiation data at doses that were equivalent to less than 0.5 dpa of the He irradiation. For Kr irradiation, the measured M was multiplied by 0.89 to correct for the 12% higher calculated results relative to the uniform damage profile results. As was done for the Ne data, Eq. (16) was applied to the Kr data when the doses equivalent to the He irradiation were less than 0.5 dpa. Figure 8 shows the amount of Au depletion measured as a function of dose for the four different 1.8-MeV ion irradiations. The efficiencies for producing freely migrating defects determined for the 1.8-MeV ^{1}H, ^{20}Ne, and ^{84}Kr ions relative to the 1.8-MeV ^{4}He irradiation were 1.9, 0.14, and 0.11, respectively.

IV. DISCUSSION

A strong decrease in the relative efficiency for producing freely migrating defects in Cu-Au alloys is clearly seen when going from light- to heavy-ion irradiations. Qualitatively this is to be expected, as has been discussed previously in Refs. 1 and 6. The fraction of defects which become free to migrate depends strongly on whether they are produced as isolated Frenkel pairs or in cascade regions that have locally high defect densities. Because dpa calculations provide no information on whether defects are produced in cascade events or as isolated Frenkel pairs, dpa calculations cannot be expected to serve as a reliable basis for correlating microstructural changes produced at elevated temperatures by different irradiation particles.

A partial description of the fraction of defects produced in cascades relative to those produced as isolated Frenkel pairs can, however, be inferred from the calculated distribution of energies with which the primary

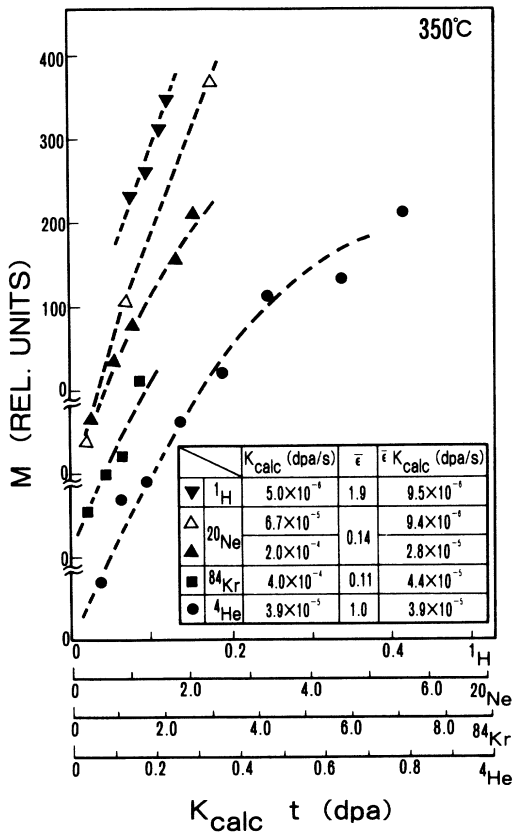

FIG. 8. Amount of segregation measured for the different ion irradiations. $\bar{\epsilon}$ is the efficiency for producing freely migrating defects relative to He irradiation. For Kr irradiation, the effect of a nonuniform damage-rate distribution has been corrected as described in the text. Abscissas represent the calculated doses. They have been adjusted using the determined efficiencies so that the "effective dose" for all the ions becomes equal.

knock-on atoms (PKA) recoil. This distribution of recoil energies is called the primary-recoil spectrum for an irradiation, and it can be calculated using standard computer codes. Since we are, in fact, concerned with describing the spatial distribution of the defects that are produced, the function of fundamental interest is the primary-recoil spectrum weighted by the total number of Frenkel pair defects produced by each primary recoil. To obtain this weighted-average recoil spectrum, which is discussed in detail in Ref. 1, we need to calculate, $W(P)$, the fraction of defects produced by all primary-recoil atoms with energy less than P. $W(P)$ is defined as[1]

$$W(P)=\frac{1}{\nu(E)}\int_{P_{\min}}^{P}\frac{d\sigma(E,P')}{dP'}\nu(P')dP' , \tag{17}$$

where

$$\nu(E)=\int_{P_{\min}}^{P_{\max}}\frac{d\sigma(E,P')}{dP'}\nu(P')dP' \tag{18}$$

and $d\sigma(E,P')/dP'$ is the differential cross section for a particle of energy E to produce a primary-recoil atom with energy P'. The number of Frenkel pairs produced by recoil atoms of energy P' is $\nu(P')$. A modified Kinchin-Pease expression[26] was employed to calculate the Frenkel pair production

$$\nu(P')=\begin{cases}0 & (P'<P_{\min})\\ 1 & (P_{\min}\le P'\le 2.5P_{\min})\\ \dfrac{0.8E_D(P')}{2P_{\min}} & (2.5P_{\min}<P')\end{cases}, \tag{19}$$

where $E_D(P')$ is the calculated damage energy, i.e., the energy deposited into nuclear collisions. Figure 9 shows $W(P)$ calculated using PINTO for the four ion irradiations used in the present study. The PKA median energy, $P_{1/2}$, which is defined as

$$\int_{P_{\min}}^{P_{1/2}}\frac{d\sigma(E,P')}{dP'}\nu(P')dP'=\frac{1}{2}\int_{P_{\min}}^{P_{\max}}\frac{d\sigma(E,P')}{dP'}\nu(P')dP' \tag{20}$$

provides a useful parameter to characterize each primary-recoil spectrum. For a given irradiation particle and target, half of the defects are produced by primary-recoil atoms that receive energies above $P_{1/2}$, and half are produced by atom recoils below $P_{1/2}$. Larger values of $P_{1/2}$, therefore, imply that a greater fraction of the total number of irradiation-induced defects are produced in energetic displacement cascades. Cascade regions can be clearly identified in computer simulation studies for primary-recoil energies $\gtrsim 1$ keV. The PKA median energies calculated for 1.8-MeV, ^{1}H, ^{4}He, ^{20}Ne, and ^{84}Kr ions are 0.83, 1.7, 13, and 79 keV, respectively (see Fig. 9). Renormalizing the efficiencies for the ^{4}He, ^{20}Ne, and ^{84}Kr ions relative to the ^{1}H irradiation, the relative defect production efficiencies for the irradiations with 1.7-, 13-, and 79-keV PKA median energies are determined to be 53%, 7%, and 6%, compared to the irradiation with a 0.83-keV median energy. In Fig. 10, the relative efficiencies obtained for Cu-Au are plotted as a function of $P_{1/2}$, along with results reported previously for Ni-Si alloys.[7]

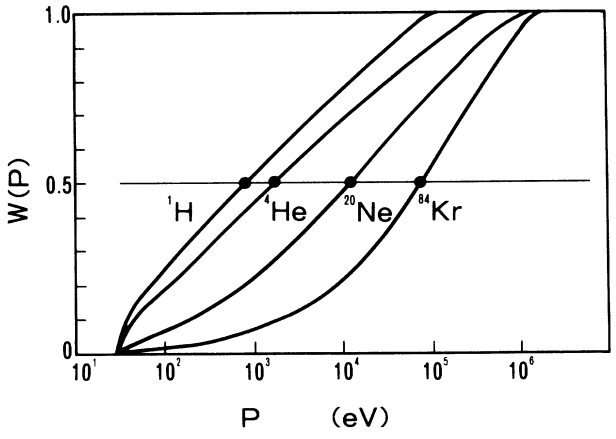

FIG. 9. Calculated fraction of defects produced by primary-recoil events of energy less than P: (1) 1.8-MeV ^{1}H, (2) 1.8-MeV ^{4}He, (3) 1.8-MeV ^{20}Ne, (4) 1.8-MeV ^{84}Kr.

The relative efficiencies obtained using Cu-Au are remarkably similar to those found previously in Ni-Si alloys. A transition from large to small efficiency values occurs at relatively low recoil energies (~ 1 keV). The relative efficiencies become constant at high recoil energies at a value of only a few percent of the light-ion results. These characteristics of the relative efficiencies for producing freely migrating defects at elevated temperatures agree qualitatively with efficiencies for generating stable defects at liquid-He temperatures obtained from measurements of irradiation-induced resistivity changes.[1] This qualitative similarity implies that the same underlying physical process, namely the production at high recoil energies of several defect pairs in close proximity to each other, is responsible for the decreases in both defect survival at low temperatures and freely migrating defect production at elevated temperatures.

However, a major quantitative difference exists between the low- and high-temperature results. The low-temperature defect survival efficiencies saturated at a value that was still approximately 40% of that found at the lowest primary-recoil energy. In contrast, the apparent limiting value for the freely migrating defect production efficiencies (Fig. 10) at elevated temperatures is considerably less, only a few percent of the value found at the lowest primary-recoil energy. Defect interactions within energetic cascade events are responsible for both effects. However, these interactions apparently have a much larger influence on the net production of freely migrating defects.

In comparing results from the two different types of experiments, it is important to note that temperature is not the only, or even the main difference, between them. The two techniques, in fact, measure fundamentally different quantities. Resistivity measurements monitor the total number of defects that survive the brief cascade events during irradiation at low temperatures, whereas the RIS results measure only those defects that become free to migrate after they escape their parent cascade, i.e., some fraction of the resistivity result. The observation that the elevated-temperature efficiencies decrease to considerably lower values than the resistivity measurements implies that the fraction of freely migrating defects is also inversely related to the fraction of defects produced in cascade events. That is, defect interactions within cascades cause the fraction of freely migrating defects to decrease with increasing average recoil energy even faster than these interactions decrease the total number of generated defects.

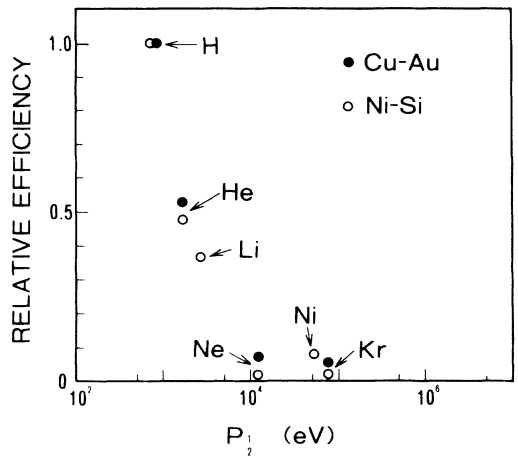

FIG. 10. Relative efficiencies for producing freely migrating defects plotted as a function of the PKA median energy.

Muroga *et al.* have performed computer simulations of cascade annealing using the MARLOWE and DAIQUIRI programs.[27] Cascade production was simulated using MARLOWE to form a nascent cascade, then annealing was simulated for about 4×10^{-6} s at 300 K using DAIQUIRI. By comparing the number of Frenkel pairs which survive athermal close-pair recombination and clustering during cascade formation, and the number of single interstitials which survive short-term annealing after the cascade has formed, they found that only a small fraction ($\sim 10\%$) of single interstitials survived short-term annealing for heavy ions as compared to light ions. Their results, therefore, also indicate that the difference between resistivity measurements at low temperatures and RIS measurements at high temperatures can be attributed to the high spatial correlation of defects produced in energetic displacement cascades.

Irradiation-induced sinks compete with the surface for segregating alloying elements. If more internal sinks are introduced during heavy-ion irradiation, more defects annihilate at sinks and consequently RIS to the near-surface region is suppressed. Hence, an apparent alternative explanation for the large reduction in efficiency for larger recoil energies is that the irradiation-induced internal sink structure dominates defect annihilation during the Ne and Kr runs. As shown in Sec. II [Eqs. (6) and (7)], any differences in the dominant defect loss mechanism will be manifested as a change in the measured dose-rate dependence of the segregation. The role of irradiation-induced defect sinks in reducing the efficiencies obtained for the heavy-ion irradiations was found to be negligible in the case of Ni-Si alloys. To examine this question further for Cu-Au, RIS measurements were made at two different dose rates, calculated to be 6.7×10^{-5} and 2.0×10^{-4} dpa/s, using Ne ions. As seen in Fig. 8, a clear dependence on dose rate was observed.

To evaluate the segregation rate ratio, R, using Eq. (11), quadratic polynomial fitting is preferred because the data points lie in the nonlinear, dose-dependent region. Since only three data points are available for the irradiation at a dose rate of 6.7×10^{-5} dpa/s, the quadratic polynomial fitting has no remaining constraint. Nevertheless, R determined from Eq. (11) is 1.5, which is quite close to the 1.3 predicted for the recombination-limited regime. Therefore, the large decrease in efficiency for Ne irradiations is, as was found for Ni-Si, apparently not due to any difference in the irradiation-induced sink structure between light and heavy ions.

The dominant mode of preferential atom transport that drives the observed RIS is different for Cu-Au and Ni-Si alloys. Preferential transport of solvent atoms by the interstitial flux is responsible for RIS in Cu-Au alloys,

TABLE III. Comparison of RIS kinetics in Cu-Au and Ni-Si alloys.

	Cu-Au alloys	Ni-Si alloys
Solute segregation at sink	depletion	enrichment
Measure of RIS	number of Au atoms in depleted layer (M)	Ni_3Si layer thickness (y)
Dominant RIS mode	solvent interstitials	interstitial-solute complexes
Temperature range	300–500 °C	350–700 °C
Dose dependence	linear (at low doses) to constant (at high doses)	parabolic
Dose rate dependence	$\frac{dM}{d\phi} \propto K_0^{-1/4}$ (at low temperature)	$\frac{dy}{d(\phi^{1/2})} \propto \begin{cases} K_0^{-1/4} & \text{(low temp.)} \\ \text{const} & \text{(high temp.)} \end{cases}$
Temperature dependence	peak at intermediate temperatures	$y \propto \begin{cases} \exp(-H_V^M/4kT) & \text{(low temp.)} \\ \exp(H_V^F/2kT) & \text{(high temp.)} \end{cases}$

whereas preferential transport via interstitial-solute complexes apparently plays the major role in Ni-Si alloys.[3–5] Near-surface solute enrichment occurs in Ni-Si during irradiation, while the same region is depleted of solute in Cu-Au. Consequently, the kinetics of RIS in the two alloy systems are quite different, as summarized in Table III. Furthermore, RIS induces second-phase precipitates in Ni-Si, but not in Cu-Au. The excellent agreement in relative efficiencies obtained for these two different alloys, therefore, suggests that the results constitute a general basis for correlating irradiation-induced microstructural changes at elevated temperatures in a wide variety of alloy systems and irradiation environments.

V. SUMMARY

In this paper, the kinetics of RIS in Cu-Au alloys and the procedure to extract the relative efficiencies for producing freely migrating defects from measurements of RIS are described. In excellent quantitative agreement with the results found previously for Ni-Si alloys, the relative efficiencies for producing freely migrating defects at elevated temperatures determined for the Cu-Au alloys exhibit a strong decrease with increasing primary-recoil energy. The relative efficiencies saturate at high recoil energies at a value which is only a few percent of that obtained at low recoil energies. The RIS kinetics and point-defect properties are quite different in the two alloy systems. The similarity in relative efficiencies for Ni-Si and Cu-Au alloys, therefore, indicates that these results constitute a general basis for correlating irradiation-induced microstructural changes at elevated temperatures in a wide variety of alloys and irradiation environments.

ACKNOWLEDGMENTS

The authors are grateful to Dr. N. Q. Lam for many useful discussions and providing a computer program of the Johnson-Lam RIS model. The expert technical assistance of P. M. Baldo and L. J. Thompson are also gratefully acknowledged. One of us (T.H.) wishes to express his gratitude to Dr. P. R. Okamoto and Dr. L. E. Rehn for their kind hospitality and stimulating discussions during his stay at Argonne National Laboratory. Work supported by the U.S. Department of Energy, Basic Energy Sciences–Materials Sciences, under Contract No. W-31-109-Eng-38.

[1]See, for example, R. S. Averback, R. Benedek, and K. L. Merkle, Phys. Rev. B **18**, 4156 (1978).

[2]P. R. Okamoto, L. E. Rehn, and R. S. Averback, J. Nucl. Mater. **108/109**, 319 (1982).

[3]Review is available in P. R. Okamoto and L. E. Rehn, J. Nucl. Mater. **83**, 2 (1972).

[4]R. S. Averback, L. E. Rehn, W. Wagner, H. Wiedersich, and P. R. Okamoto, Phys. Rev. B **28**, 3100 (1983).

[5]L. E. Rehn and P. R. Okamoto, in *Phase Transformations During Irradiation,* edited by F. V. Nolfi, Jr. (Applied Science, Essex, England, 1983), Chap. 8.

[6]R. S. Averback, L. E. Rehn, W. Wagner, and P. Ehrhart, J. Nucl. Mater. **118**, 83 (1983).

[7]L. E. Rehn, P. R. Okamoto, and R. S. Averback, Phys. Rev. B **30**, 3073 (1984).

[8]M. A. Kirk and T. H. Blewitt, Metall. Trans. A **9**, 1729 (1978).

[9]T. Hashimoto, L. E. Rehn, and P. R. Okamoto, American Society for Testing and Materials Special Technical Publication **955**, 700 (1987).

[10]PINTO was written by R. Benedek, ANL, from whom copies

can be obtained; details can be found in Ref. 1.
[11]J. R. Manning, Phys. Rev. **116**, 819 (1959); A. D. LeClaire and A. B. Lidiard, Philos. Mag. **1**, 518 (1956).
[12]K. Hirano, in *Point Defects and Defect Interactions in Metals,* edited by J. Takamura, M. Doyama, and M. Kiritani (University of Tokyo Press, Tokyo, 1982), p. 541.
[13]Detailed discussions can be found in Ref. 5, pp. 279–285.
[14]R. A. Johnson and N. Q. Lam, Phys. Rev. B **13**, 4364 (1976).
[15]N. Q. Lam and S. J. Rothman, Radiat. Eff. **23**, 53 (1974).
[16]R. S. Averback, L. J. Thompson, Jr., J. Moyle, and M. Shalit, J. Appl. Phys. **53**, 1342 (1982).
[17]J. F. Ziegler, R. F. Lever, and J. K. Hirvonen, in *Ion Beam Surface Layer Analysis,* edited by O. Meyer, G. Linker, and K. Koppler (Plenum, New York, 1976), p. 163.
[18]J. P. Biersack and L. G. Haggmark, Nucl. Instrum. Methods **174**, 257 (1980).
[19]N. Q. Lam, P. R. Okamoto, and R. A. Johnson, J. Nucl. Mater. **78**, 408 (1978).
[20]P. H. Dederichs, C. Lehmann, H. R. Schober, A. Scholz, and R. Zeller, in *Properties of Atomic Defects in Metals,* edited by N. L. Peterson and R. W. Siegel (North-Holland, Amsterdam, 1977), p. 176.
[21]A. Seeger and H. Mehrer, in *Vacancies and Interstitials in Metals,* edited by A. Seeger *et al.* (North-Holland, Amsterdam, 1970), p. 1.
[22]W. Schilling, J. Nucl. Mater. **69/70**, 465 (1978).
[23]R. W. Siegel, in *Point Defects and Defect Interactions in Metals,* edited by J. Takamura, M. Doyama, and M. Kiritani (University of Tokyo Press, Tokyo, 1982), p. 533.
[24]R. W. Siegel, in *Positron Annihilation,* edited by P. G. Coleman, S. C. Sharma, and L. M. Diana (North-Holland, Amsterdam, 1982), p. 351.
[25]F. W. Young, J. Nucl. Mater. **69/70**, 310 (1978).
[26]M. J. Norgett, M. T. Robinson, and I. M. Torrens, Nucl. Eng. Des. **33**, 50 (1974).
[27]T. Muroga and S. Ishino, J. Nucl. Mater. **117**, 36 (1983).